

Mixed eigenstates in the Dicke model: Statistics and power-law decay of the relative proportion in the semiclassical limit

Qian Wang 

*CAMTP-Center for Applied Mathematics and Theoretical Physics, University of Maribor,
Mladinska 3, SI-2000 Maribor, Slovenia, European Union
and Department of Physics, Zhejiang Normal University, Jinhua 321004, China*

Marko Robnik 

*CAMTP-Center for Applied Mathematics and Theoretical Physics, University of Maribor, Mladinska 3,
SI-2000 Maribor, Slovenia, European Union*



(Received 20 September 2023; accepted 5 February 2024; published 28 February 2024)

How the mixed eigenstates vary when approaching the semiclassical limit in mixed-type many-body quantum systems is an interesting but still less known question. Here, we address this question in the Dicke model, a celebrated many-body model that has a well defined semiclassical limit and undergoes a transition to chaos in both quantum and classical cases. Using the Husimi function, we show that the eigenstates of the Dicke model with mixed-type classical phase space can be classified into different types. To quantitatively characterize the types of eigenstates, we study the phase space overlap index, which is defined in terms of the Husimi function. We look at the probability distribution of the phase space overlap index and investigate how it changes with increasing system size, that is, when approaching the semiclassical limit. We show that increasing the system size gives rise to a power-law decay in the behavior of the relative proportion of mixed eigenstates. Our findings shed more light on the properties of eigenstates in mixed-type many-body systems and suggest that the principle of uniform semiclassical condensation of Husimi functions should also be valid for many-body quantum systems.

DOI: [10.1103/PhysRevE.109.024225](https://doi.org/10.1103/PhysRevE.109.024225)

I. INTRODUCTION

Characterizing and understanding quantum chaos in many-body quantum systems through the properties of eigenstates is a widely studied topic. Even though it has been explored since the birth of quantum mechanics, the close connection between chaos and the questions that arise in recent experimental and theoretical studies has led to a revival in studying various features of chaotic eigenstates, such as their entanglement entropy [1–3], delocalization or localization [4–9], scarring [10–13], and multifractality [14–16] as well. Unlike the strongly chaotic (ergodic) systems, the properties of eigenstates in the mixed-type many-body systems having regular regions coexisting with chaotic regions in the classical phase space are less commonly explored [17,18], despite the fact that mixed-type behavior is more generic.

In studying the single-particle systems, it has been demonstrated that the classical counterparts of the mixed-type quantum systems are generally associated with mixed-type phase space with coexistence of regular and chaotic motions. Based on this fact, Percival was the first to suggest that the eigenstates in mixed-type quantum systems can be divided into the chaotic and regular types [19]. After further developments performed by Berry [20,21], this suggestion became the principle of uniform semiclassical condensation of Wigner (or Husimi) functions (PUSC) [22–24]. In the ultimate semiclassical limit, various characters [25,26], in particular the spectral statistics [27–32], of mixed-type

single particle systems can be well understood by means of the PUSC. Moreover, the correctness of the PUSC for the cases that are not in the asymptotic semiclassical limit is also verified in recent works [33,34]. The evolution of the mixed eigenstates overlapping, partially, with both a regular and a chaotic region, as the semiclassical limit is approached, has been revealed. However, the situation for the many-body quantum systems is more complicated and has not yet been explored so far.

In this work, we will investigate whether and how the eigenstates of a mixed-type many-body quantum system separate into the regular and chaotic states with approaching the semiclassical limit. This requires the considered many body system to have a well defined semiclassical limit. The model we focus on is the celebrated Dicke model [35]. An advantage of the Dicke model is that it attains its semiclassical limit with increasing the system size N and, thus, allows us to define an effective Planck constant $\hbar_{\text{eff}} \simeq 1/N$. A rich variety of phases observed in the Dicke model has made it a very popular model to study different phase transitions, including thermal phase transition [36–40], nonequilibrium phase transitions [41], quantum phase transition [42–47], as well as excited state quantum phase transition [39,48–53]. In particular, both quantum and classical Dicke models allow the transition from integrability to chaos by changing certain control parameters [47,54–56]. As a consequence, it has been widely employed as a paradigmatic model for studying quantum chaos [54–60] and thermalization [61–66]. It is, therefore,

a particularly suitable many-body quantum model for our purpose, as a continuation of our previous works [8,34]. The Dicke model as a dynamical system is entirely and fundamentally different from the previously studied single-particle systems. Hence, it is far from trivial to explore whether the properties of the mixed eigenstates that are observed in the single-particle systems still hold in the Dicke model. The presence of the interactions in many-body systems indicates that a direct generalization of the conclusions from single-particle systems to many-body cases is not allowed. This means that scrutinizing the features of the mixed eigenstates in the Dicke model is required to investigate how the fraction of the mixed eigenstates evolves when approaching the semiclassical limit.

By carrying out a detailed analysis of the dependence of the degree of chaos on the control parameters for both classical and quantum models, we determine our studied parameter regions. We demonstrate how to identify the types of the eigenstates by comparing their Husimi functions with the classical Poincaré section. To quantitatively describe different types of eigenstates, we utilize the phase space overlap index, which is defined in terms of eigenstates' Husimi functions and has been proved as a valuable tool to quantify eigenstates properties. We show that the statistics of the phase space overlap index is approximately captured by double peak distribution with two peaks close to its extreme values, corresponding to entirely regular and chaotic eigenstates. Moreover, we find that the relative proportion of the mixed eigenstates follows the power-law decay as the semiclassical limit is approached, by increasing the system size. These results are consistent with the ones revealed in the single-particle systems, suggesting the validity of the PUSC for many-body quantum systems.

The rest of the article is structured as follows. In Sec. II, we introduce the Dicke model. Section II A is devoted to the analysis of the semiclassical Dicke model and shows how chaos develops when varying either the control parameter or the energy of the system. In Sec. II B, we discuss the emergence of chaos in the quantum Dicke model by means of the statistics of level spacing ratio. Section III reports our main results of this work. In Sec. III A, the Husimi function of an individual eigenstate is defined and employed to illustrate different types of the eigenstates. The definition of the phase space overlap index and its distribution, as well as the variation of the relative proportion of mixed eigenstates with system size, are analyzed in Sec. III B. We finally summarize our findings and conclude in Sec. IV.

II. DICKE MODEL

In this section, in addition to giving a brief review of the basic features of the Dicke model, we also discuss how to characterize the transition to chaos in both parameter and energy spaces using various chaotic detectors, such as level spacing ratio statistics, the largest and phase space averaged Lyapunov exponents. The results obtained through these analyses not only enable us to determine parameter and energy ranges of interest, but also provide more insights into the properties of the Dicke model.

As the simplest atom-field system, the Dicke model [35] consists of an ensemble of N spin-1/2 atoms interacting with a single electromagnetic mode within a cavity, and its Hamiltonian reads [47] (setting $\hbar \equiv 1$)

$$H = \omega a^\dagger a + \omega_0 J_z + \frac{2\lambda}{\sqrt{N}} J_x (a^\dagger + a), \quad (1)$$

where ω is the frequency of the cavity mode, ω_0 denotes the energy splitting of atoms, and λ represents the atom-cavity coupling strength. Here, a (a^\dagger) is the usual bosonic annihilation (creation) operator, while $\mathbf{J} = (J_x, J_y, J_z)$ are the collective pseudospin operators describing N spin-1/2 atoms. These pseudospin operators fulfill the SU(2) commutation relations.

The Hamiltonian (1) conserves the total spin operator \mathbf{J}^2 , so that the Hilbert space can be separated into different subspaces according to the eigenvalues of \mathbf{J}^2 . Our study will be restricted to the subspace with $j = N/2$ and the Hilbert space dimension $\mathcal{D}_{\mathcal{H}} = (N+1)(\mathcal{N}_{\text{trc}}+1)$. Here, \mathcal{N}_{trc} denotes the truncation number of the bosonic basis. Moreover, since the parity operator $\Pi = e^{i\pi(a^\dagger a + J_z + j)}$ is also a conserved quantity, $[H, \Pi] = 0$, one can further divide the Hilbert space into even- and odd-parity blocks. In this work, we focus on the even-parity sector with even j . As a result, the dimension of the Hilbert space is $\mathcal{D}_{\mathcal{H}}^e = (N/2+1)(\mathcal{N}_{\text{trc}}+1) - \mathcal{N}_{\text{trc}}/2$. To guarantee the convergence of the numerical results, the value of \mathcal{N}_{trc} should be sufficiently large. We have carefully checked that the results obtained in this work are converged for our chosen values of \mathcal{N}_{trc} , whose maximal value was 300.

It was known that the ground state of the model undergoes a second-order quantum phase transition at the critical point $\lambda_c = \sqrt{\omega\omega_0}/2$, which separates the normal phase with $\lambda < \lambda_c$ from the super-radiant phase with $\lambda > \lambda_c$ [47]. Apart from the ground state quantum phase transition, the excited energy spectrum of the system also exhibits an excited state quantum phase transition [67–69] into the super-radiant phase [39,49–53,70]. In particular, both ground and excited state quantum phase transitions are associated with the onset of classical and corresponding quantum chaos [46–50].

A. Chaos in semiclassical system

In the semiclassical limit with $N \rightarrow \infty$, the Hamiltonian (1) turns into its classical counterpart. To obtain the effective classical Hamiltonian, we utilize the Glauber and Bloch coherent states [71,72], which are, respectively, defined as

$$\begin{aligned} |\alpha\rangle &= e^{|\alpha|^2/2} e^{\alpha a^\dagger} |0\rangle, \\ |\xi\rangle &= \frac{1}{(1+|\xi|^2)^j} e^{\xi J_+} |j, -j\rangle. \end{aligned} \quad (2)$$

Here, α, ξ are the complex parameters, $|0\rangle$ is the bosonic field vacuum, and $|j, -j\rangle$ is the ground state of the atomic sector. Then, according to the properties of the coherent states, it is straightforward to find the following relations:

$$\begin{aligned} \langle \alpha | a^\dagger a | \alpha \rangle &= |\alpha|^2, \\ \langle \xi | J_x | \xi \rangle &= j \left(\frac{\xi + \xi^*}{1 + |\xi|^2} \right), \\ \langle \xi | J_z | \xi \rangle &= -j \left(\frac{1 - |\xi|^2}{1 + |\xi|^2} \right). \end{aligned} \quad (3)$$

The classical Hamiltonian is the expectation of the quantum Hamiltonian (1) in the tensor product of the coherent states, $|\text{CS}\rangle = |\alpha\rangle \otimes |\xi\rangle$ [56,73,74]. Using above relations, one can easily find that the classical Hamiltonian can be written as

$$\begin{aligned} \mathcal{H}_c &= \frac{\langle \text{CS} | H | \text{CS} \rangle}{j} \\ &= \omega \frac{|\alpha|^2}{j} - \omega_0 \left(\frac{1 - |\xi|^2}{1 + |\xi|^2} \right) + \frac{2\lambda}{\sqrt{N}} (\alpha^* + \alpha) \left(\frac{\xi + \xi^*}{1 + |\xi|^2} \right). \end{aligned} \quad (4)$$

To express \mathcal{H}_c in terms of the classical canonical variables, we parametrize α and ξ as follows [10,53,73]:

$$\alpha = \sqrt{\frac{j}{2}} (q_1 + ip_1), \quad \xi = \frac{q_2 + ip_2}{\sqrt{4 - p_2^2 - q_2^2}}, \quad (5)$$

where $(p_1, q_1) \in \mathbb{R}^2$ are the canonical variables for the bosonic sector, while $(p_2, q_2) \in \mathbb{R}^2$ and $p_2^2 + q_2^2 \leq 4$ denote the atomic sector canonical variables [75]. Finally, inserting the parametrized α and ξ into Eq. (4), after some algebra, the classical Hamiltonian is given by

$$\begin{aligned} \mathcal{H}_c &= \frac{\omega}{2} (p_1^2 + q_1^2) + \frac{\omega_0}{2} (p_2^2 + q_2^2) \\ &\quad + \lambda q_1 q_2 \sqrt{4 - p_2^2 - q_2^2} - \omega_0. \end{aligned} \quad (6)$$

The classical system is described by the canonical variables $\mathbf{x} = (q_1, q_2, p_1, p_2) \in \mathbb{R}^4$, meaning that the classical phase space is four dimensional. From the classical Hamiltonian (6), the classical equations of motion are given by

$$\begin{aligned} \dot{q}_1 &= \frac{\partial \mathcal{H}_c}{\partial p_1} = \omega p_1, & \dot{q}_2 &= \frac{\partial \mathcal{H}_c}{\partial p_2} = \omega_0 p_2 - \frac{\lambda q_1 q_2 p_2}{\sqrt{4 - p_2^2 - q_2^2}}, \\ \dot{p}_1 &= -\frac{\partial \mathcal{H}_c}{\partial q_1} = -\omega q_1 - \lambda q_2 \sqrt{4 - p_2^2 - q_2^2}, \\ \dot{p}_2 &= -\frac{\partial \mathcal{H}_c}{\partial q_2} = -\omega_0 q_2 - \lambda q_1 \sqrt{4 - p_2^2 - q_2^2} + \frac{\lambda q_1 q_2^2}{\sqrt{4 - p_2^2 - q_2^2}}, \end{aligned} \quad (7)$$

associated with the initial condition $\mathbf{x}_0 = (q_{1,0}, q_{2,0}, p_{1,0}, p_{2,0})$.

It is known that the classical Dicke model undergoes a transition from integrability to chaos when increasing either the coupling strength with fixed energy or the energy at fixed λ which satisfies $\lambda > \lambda_c$. To see this, we exploit the Poincaré sections to qualitatively demonstrate how chaos emerges as the coupling strength or energy varies. Here, we define the Poincaré section for a given energy \mathcal{E} as the intersection of the classical trajectories with the surface that is the plane in the variables (p_2, q_2) with $p_1 = 0$ and q_1 being determined by the energy conservation condition $\mathcal{H}_c = \mathcal{E}$. By solving the quadratic equation $\mathcal{H}_c(q_1, q_2, p_1 = 0, p_2) = \mathcal{E}$, we get two

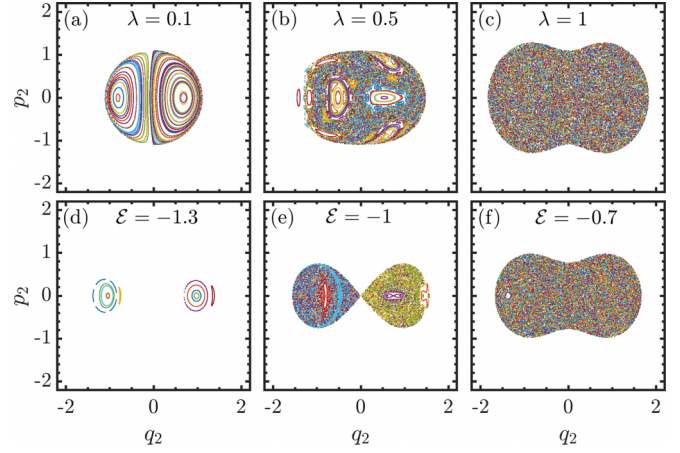


FIG. 1. Classical Poincaré sections of the system (6) in the (q_2, p_2) plane. Panels (a)–(c) show the Poincaré sections for several coupling strengths with fixed energy $\mathcal{E} = -0.4$, while (d)–(f) are the Poincaré sections for different energies with $\lambda = 0.8$. In all panels, different colors correspond to different initial conditions. Other parameters: $\omega = \omega_0 = 1$. All quantities are dimensionless.

different values of q_1 :

$$\begin{aligned} q_{1,\pm} &= -\frac{\lambda}{\omega} q_2 \sqrt{4 - p_2^2 - q_2^2} \\ &\quad \pm \sqrt{\frac{\lambda^2}{\omega^2} q_2^2 (4 - p_2^2 - q_2^2) - \omega_0 (p_2^2 + q_2^2) + 2(\omega_0 + \mathcal{E})}. \end{aligned} \quad (8)$$

Moreover, we only record the traversals with $q_1 > 0$.

The Poincaré sections for several coupling strengths with $\mathcal{E} = -0.4$ are plotted in Figs. 1(a)–1(c). At weak coupling strength, as seen in Fig. 1(a), the Poincaré section exhibits a regular structure, indicating that the system is governed by the regular dynamics. The chaotic orbits appear as the coupling strength increases, as exemplified in Fig. 1(b) for $\lambda = 0.5$ case, where the Poincaré section has complex structure with regular islands embedded in the chaotic sea. When the coupling strength is sufficiently strong, the system becomes a fully chaotic system whose Poincaré section is erratically covered by all orbits from a set of disordered points, as illustrated in Fig. 1(c). The dependence of the degree of chaos on the system energy is displayed in Figs. 1(d)–1(f), where we show the Poincaré sections for different system energies with $\lambda = 0.8$. A transition of the Poincaré section from the regular pattern to a globally chaotic sea is clearly visible. Hence, the level of chaos in the Dicke model depends on both the coupling strength and the system energy.

To quantitatively analyze the development of chaos depending upon the strength of coupling λ and the system energy \mathcal{E} , we consider the maximal Lyapunov exponent, which measures the rate of exponential separation between two infinitesimally close orbits. For the Dicke model, it can be calculated as [56,76]

$$\Lambda_m = \lim_{t \rightarrow \infty} \lim_{\|\delta \mathbf{x}_0\| \rightarrow 0} \frac{1}{t} \ln \frac{\|\Omega(t) \cdot \delta \mathbf{x}_0\|}{\|\delta \mathbf{x}_0\|}, \quad (9)$$

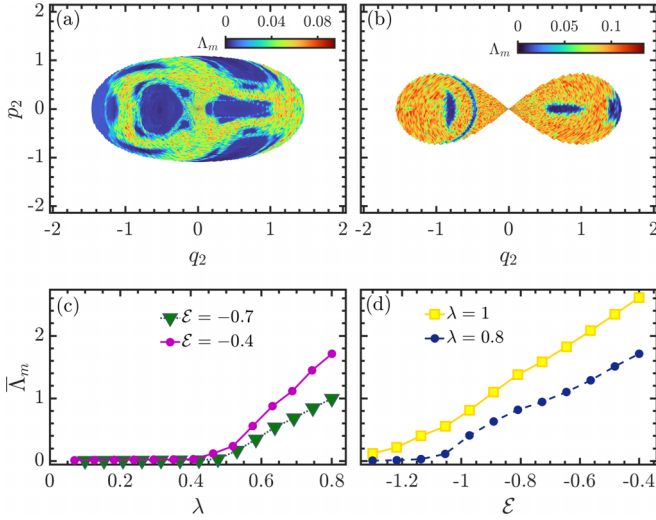


FIG. 2. Maximal Lyapunov exponent, Λ_m , as a function of q_2 and p_2 for (a) $\lambda = 0.5$, $\mathcal{E} = -0.4$ and (b) $\lambda = 0.8$, $\mathcal{E} = -1$. The maximal Lyapunov exponent is calculated on a grid of 150×150 initial conditions, and each has evolved up to time $t = 1000$. (c) Phase space averaged maximal Lyapunov exponent, $\bar{\Lambda}_m$, as a function of λ for different energies. (d) $\bar{\Lambda}_m$ as a function of energy for different coupling strengths λ . Other parameters: $\omega = \omega_0 = 1$. All quantities are dimensionless.

where $\delta \mathbf{x}_0 = (\delta q_{1,0}, \delta q_{2,0}, \delta p_{1,0}, \delta p_{2,0})^T$ is the initial deviation between two given orbits and $\Omega(t)$ is the fundamental matrix [76], determined by the equation

$$\dot{\Omega}(t) = [\mathbf{J}_4 \cdot D^2 \mathcal{H}_c(\mathbf{x}(t))] \cdot \Omega(t). \quad (10)$$

Here, the initial condition is $\Omega(0) = \mathbb{I}_4$ with \mathbb{I}_4 being the 4×4 identity matrix, while \mathbf{J}_4 and $D^2 \mathcal{H}_c(\mathbf{x}(t))$ are 4×4 matrices given by

$$\mathbf{J}_4 = \begin{pmatrix} \mathbf{0}_2 & \mathbb{I}_2 \\ -\mathbb{I}_2 & \mathbf{0}_2 \end{pmatrix}, \quad [D^2 \mathcal{H}_c(\mathbf{x}(t))]_{i,j} = \left. \frac{\partial^2 \mathcal{H}_c}{\partial x_i \partial x_j} \right|_{\mathbf{x}(t)}, \quad i, j = 1, 2, \dots, 4, \quad (11)$$

with $\mathbf{0}_2$ being the 2×2 zero matrix and $\mathbf{x}(t)$ being the solution of the classical equations of motion (7) at time t .

The maximal Lyapunov exponent as a function of p_2 and q_2 for two different combinations of energy \mathcal{E} and coupling strength λ are plotted in Figs. 2(a) and 2(b), respectively. A comparison with the Poincaré sections in Figs. 1(b) and 1(e) unveils that the regular and chaotic regions are clearly distinguished by $\Lambda_m \approx 0$ and $\Lambda_m > 0$, as expected. A further observation of the exhibited behavior of Λ_m is that it increases as the energy and coupling strength are increased.

The dependence of the level of chaos on the energy and coupling strength can be quantitatively captured by the phase space averaged maximal Lyapunov exponent, which in this case is also known as the Kolmogorov-Sinai entropy [77] and is defined as

$$\bar{\Lambda}_m = \int dS \Lambda_m, \quad (12)$$

where $dS = r dr d\theta$ is the phase space area element in polar coordinates. In Fig. 2(c), the variation of $\bar{\Lambda}_m$ with coupling strength λ is shown for different energies. For the system with $\lambda \lesssim 0.4$, $\bar{\Lambda}_m = 0$, regardless of the energy, suggesting the regular dynamics of the system. As soon as $\lambda \gtrsim 0.5$, $\bar{\Lambda}_m$ starts to increase with increasing λ independently of the energy, indicating the development of chaos in the system. It is remarkable that this happens approximately at the critical point, λ_c , of the quantum phase transition. Additionally, it is obvious that the larger the energy is, the faster $\bar{\Lambda}_m$ grows. Besides, with increased system energy the onset of chaos happens at smaller value of the coupling strength. These observations indicate that the system energy strongly affects the degree of chaos. The impact of energy on the level of chaos is clearly unveiled in Fig. 2(d), where we plot $\bar{\Lambda}_m$ as a function of energy \mathcal{E} for different values of λ . One can see that $\bar{\Lambda}_m$ exhibits an obvious transition from very tiny values to large values with increasing energy. We also note that the transition to chaos shifts to lower energy with increasing the strength of coupling. It is worth mentioning that the above features of $\bar{\Lambda}_m$ are consistent with the Poincaré sections shown in Fig. 1.

B. Chaos in quantum system

Let us now turn to chaotic transition in the quantum model (1). The presence of quantum chaos can be diagnosed by numerous indicators, including spectral and eigenstates statistics [78–83], various dynamical probes [83–85], and different complexities [86–92], to mention a few. Here, we focus on the distribution of level spacing ratios, defined as [93,94]

$$r_n = \min\left(\delta_n, \frac{1}{\delta_n}\right), \quad (13)$$

where $\delta_n = s_n/s_{n+1}$ with $s_n = E_{n+1} - E_n$ being the consecutive level spacing for ordered energy levels $E_n < E_{n+1}$ of the Hamiltonian (1). As investigating the spacing ratio distribution is free from the need to perform the unfolding procedure for the energy spectrum, it turns out to be the most widely used chaos indicator for studying quantum many-body chaos [15,18,95–98]. Another advantage of using r_n instead of s_n as chaos indicator is that the support of the distribution of r_n is bounded, that is $r_n \in [0, 1]$.

The distribution of r_n for chaotic systems that belong to the Gaussian orthogonal ensemble (GOE) is given by [18,94],

$$P_{\text{GOE}}(r) = \frac{2}{Z_{\text{GOE}}} \frac{r + r^2}{(1 + r + r^2)^{5/2}}, \quad (14)$$

where $Z_{\text{GOE}} = 8/27$ is the normalization constant. For integrable systems, uncorrelated eigenvalues exhibiting Poisson statistics, we have [94]

$$P_P(r) = \frac{2}{(1+r)^2}. \quad (15)$$

A prominent feature of the chaotic spectra is level repulsion characterized by $P_{\text{GOE}}(0) = 0$, in contrast to Poisson spectra with $P_P(0) \neq 0$.

In Figs. 3(a) and 3(b), we show the ratio distribution $P(r)$ for two different values of λ with system size $N = 60$. The distribution $P(r)$ in Fig. 3(a) for small λ is well captured by the Poisson case, in agreement with the classical regular dynamics

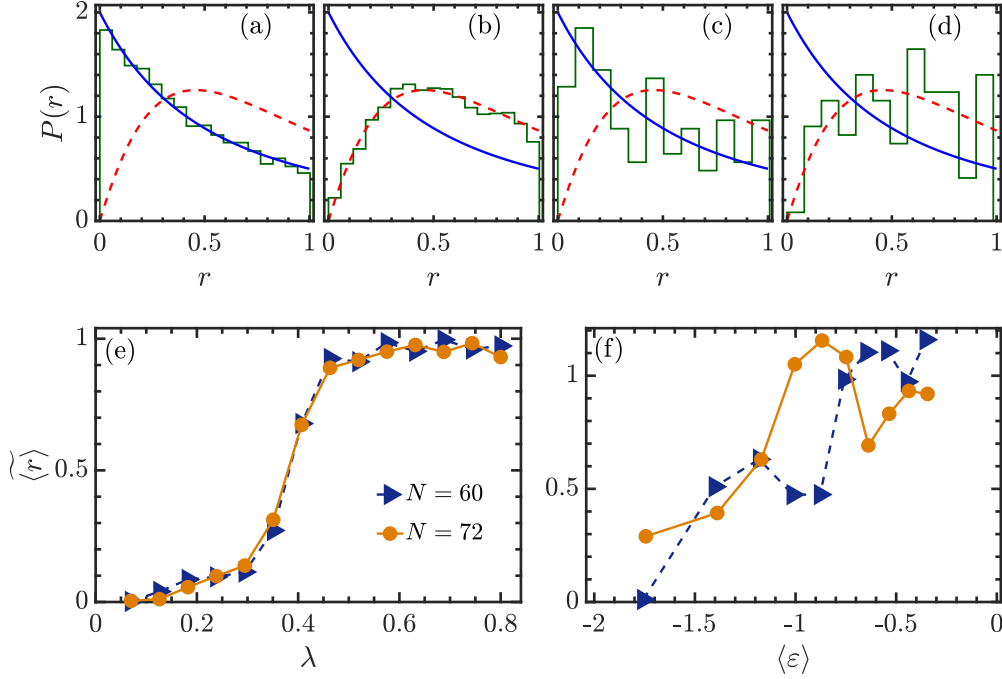


FIG. 3. (a)–(b) Level spacing ratio distribution $P(r)$ for (a) $\lambda = 0.1$ and (b) $\lambda = 1$ with $N = 2j = 60$. (c) and (d) $P(r)$ for different energy intervals: (c) $\varepsilon_n \in [\varepsilon_0, \varepsilon_{149}]$ and (d) $\varepsilon_n \in [\varepsilon_{244}, \varepsilon_{393}]$, with $N = 2j = 60$ and $\lambda = 1$. Here, $\varepsilon_n = E_n/j$ is the n th rescaled eigenenergy with $n = 0$ corresponding to the ground state. The red dashed and blue solid curves in panels (a)–(d) are P_{GOE} and $P_P(r)$, respectively. (e) Rescaled average level spacing ratio, $\langle \widetilde{r} \rangle$, as a function of coupling strength λ for several system sizes. (f) $\langle \widetilde{r} \rangle$ as a function of $\langle \varepsilon \rangle$ for the system sizes as in panel (e) with $\lambda = 1$. Here, $\langle \varepsilon \rangle = \sum \varepsilon_n/150$ is the averaged energy of each energy interval. Other parameters: $\omega = \omega_0 = 1$. The bosonic mode has been truncated at $\mathcal{N}_{trc} = 300$. All quantities are dimensionless.

exhibited in Fig. 1(a). The ratio distribution $P(r)$ for $\lambda = 1$ in Fig. 3(b) demonstrates an opposite situation, where the GOE distribution of r is clearly visible. We see again that the behavior of $P(r)$ at $\lambda = 1$ is consistent with the classical Poincaré section in Fig. 1(c). To reveal the dependence of chaos on the system energy, we consider the distribution $P(r)$ extracted from energy levels within a certain energy interval, as was done in Refs. [15,18]. The energy interval in our study is an interval between ε_n and ε_{n+149} with $\varepsilon_n = E_n/j$ being the n th rescaled eigenenergy. We plot $P(r)$ for two representative energy intervals $\varepsilon_n \in [\varepsilon_0, \varepsilon_{149}]$ and $\varepsilon_n \in [\varepsilon_{244}, \varepsilon_{393}]$ in Figs. 3(c) and 3(d), respectively. Here, ε_0 denotes the rescaled ground state energy. It can be clearly seen that the ratio distribution $P(r)$ is close to the Poisson distribution $P_P(r)$ for the lowest energy levels, while it turns to follow the GOE distribution $P_{GOE}(r)$ for the energy levels at high energy. In particular, $P(r=0)$ exhibits an obvious transition from $P(r=0) \neq 0$ to $P(r=0) \approx 0$ as the energy of energy interval is increased.

A more popular quantity that has been employed to detect the presence of quantum chaos is the mean spacing ratio, defined as $\langle r \rangle = \int_0^1 rP(r)dr$. It was known that $\langle r \rangle$ interpolates between two extreme values $\langle r \rangle_P = 2 \ln 2 - 1 \approx 0.38629$ and $\langle r \rangle_{GOE} = 4 - 2\sqrt{3} \approx 0.53590$, corresponding to Poisson and GOE distributions, respectively [94]. This leads to the definition of rescaled mean spacing ratio [97],

$$\langle \widetilde{r} \rangle = \frac{|\langle r \rangle - \langle r \rangle_P|}{\langle r \rangle_{GOE} - \langle r \rangle_P}. \quad (16)$$

It varies in the interval $\langle \widetilde{r} \rangle \in [0, 1]$. For integrable systems with Poisson distribution, we have $\langle \widetilde{r} \rangle = 0$, while chaotic systems with GOE distribution give rise to $\langle \widetilde{r} \rangle = 1$.

The variation of $\langle \widetilde{r} \rangle$ as a function of coupling strength λ for several system sizes is plotted in Fig. 3(e). We see that the overall behavior of $\langle \widetilde{r} \rangle$ as a function of λ is almost unaffected by varying the system size. Regardless of the system size, $\langle \widetilde{r} \rangle$ exhibits a rapid growth from small values to the values around 1 in the region $\lambda \in [0.35, 0.55]$. Again, it is remarkable that this is close to the critical coupling strength, λ_c , of the quantum phase transition. Thus, the quantum system undergoes a crossover from integrability to chaos with increasing the strength of coupling, in agreement with the behavior of $P(r)$ observed in Figs. 3(a) and 3(b). On the other hand, the dependence of $\langle \widetilde{r} \rangle$ on the system energy is shown in Fig. 3(f), where we display how $\langle \widetilde{r} \rangle$ evolves for different energy intervals and system sizes with fixed λ . The overall increasing behavior of $\langle \widetilde{r} \rangle$ as the energy interval moves to high energy levels confirms that the degree of chaos in the Dicke model can be enhanced by increasing the system energy. As a final remark of this section, we would like to point out that the behavior of $\langle \widetilde{r} \rangle$ coincides with $\overline{\Lambda}_m$, suggesting a good quantum-classical correspondence.

III. OVERLAP INDEX IN CLASSICAL PHASE SPACE

The aim of this work is to analyze how the mixed eigenstates in many-body systems evolve as the semiclassical limit $N \rightarrow \infty$ is approached. To this end, we employ the celebrated Dicke model, which has a well-defined classical limit and has

been used as a prototypical model in different branches of physics. In particular, the transition to chaos exhibited by the Dicke model makes it a suitable model to study the properties of the mixed eigenstates in many-body quantum systems.

The analysis of the features of the mixed eigenstates requires one to focus on the cases that have mixed-type phase space in the semiclassical dynamics. Thus, we restrict our study in the parameter region $\lambda \in [0.45, 0.5]$ with energy $\mathcal{E} \in [-0.7, -0.5]$. A careful numerical check has verified that the classical dynamics for our considered parameters and energy regions is indeed characterized by mixed-type phase space. Moreover, following our previous works [4,33,34,99], we identify the types of eigenstates through the phase space overlap index. To this end, let us first introduce the definition of the Husimi function for an individual eigenstate.

A. Husimi function

As the Gaussian smoothing of the well-known Wigner function [100], the Husimi function [101] constitutes the simplest quasiprobability distribution of a quantum state in classical phase space and has been widely used as a powerful tool to explore various properties of quantum eigenstates [8–11,45,65,102–106]. It is usually defined as the projection of a quantum state onto the coherent state [107]. Thus, the Husimi function for the n th eigenstate, $|E_n\rangle$, of the Dicke model is given by [108,109]

$$Q_n = |\langle \text{CS} | E_n \rangle|^2, \quad (17)$$

where $|\text{CS}\rangle = |\alpha\rangle \otimes |\xi\rangle$. The normalization condition of the coherent states implies that the Husimi function can be normalized as

$$\frac{2j+1}{\pi^2} \int_{\mathbb{R}^4} \frac{d^2\alpha d^2\xi}{(1+|\xi|^2)^2} Q_n = 1, \quad (18)$$

with $j = N/2$ and $d^2w = d \text{Re}(w) d \text{Im}(w)$ ($w = \alpha, \xi$).

For Hamiltonians with two degrees of freedom, such as the Dicke model, the Husimi function Q_n in (17) has four real variables. As a consequence, it is difficult to visualize and display it. A common way to circumvent this difficulty is to study different projections or sections of the Husimi function [74,110–112]. For our purpose, we consider the Poincaré-Husimi function which is evaluated along the Poincaré surface $q_{1,+}$ defined in Eq. (8) and calculated as

$$Q_n^P(p_2, q_2) = |\langle p_1 = 0, q_1 = q_{1,+}; p_2, q_2 | E_n \rangle|^2. \quad (19)$$

Here, the energies of eigenstates are chosen to satisfy $|E_n/j - \mathcal{E}| \simeq 0$ for a certain value of \mathcal{E} , so that they correspond to a well defined classical dynamical regime (phase portrait). Now, $Q_n^P(p_2, q_2)$ is a function of two variables and its density plot provides a quite illustrative comparison to the classical Poincaré section [74,112].

The Poincaré-Husimi functions for several eigenstates with energy close to $\mathcal{E} = -0.4$ are plotted in Fig. 4. Comparing with the classical Poincaré section, which is shown in Fig. 4(e), we see that the eigenstates can be qualitatively divided into three types. The first type corresponds to the eigenstates whose Poincaré-Husimi functions are mainly located in the classical regular regions, as is evident in Figs. 4(b) and 4(f). This type of eigenstates is usually called

regular eigenstates. In contrast to the regular eigenstates, the Poincaré-Husimi functions in Figs. 4(g)–4(i) are almost fully distributed over the chaotic sea. This allows us to name this type of eigenstates the chaotic eigenstates. Apart from these two extreme cases, we still have some eigenstates, referred to as the mixed eigenstates, whose Poincaré-Husimi functions occupy both regular and chaotic regions, as exemplified in Figs. 4(a), 4(c), and 4(d). The presence of the mixed eigenstates originates from different tunneling processes between various structures in classical phase space.

A natural question about the existence of different types of eigenstates is how to quantitatively characterize them. In particular, unveiling how the relative proportion of the mixed eigenstates varies as the system approaches the semiclassical limit would improve our understanding of generic quantum systems whose classical counterpart has mixed-type phase space. For single-particle systems, our previous works [33,34] have shown that the relative proportion of the mixed eigenstates undergoes a power-law decay as the semiclassical limit is approached. But, whether this conclusion still holds in many-body quantum systems remains unknown. In the following subsection, we address the above mentioned questions in the Dicke model.

B. Phase space overlap index

As was done in Refs. [4,33,34,99], we distinguish the types of the eigenstates by means of the phase space overlap index, M , defined as the overlap of the Poincaré-Husimi function with different regions of phase space. Specifically, by employing the polar coordinates (r, θ) with $0 \leq r \leq 2$, we separate the classical phase space (q_2, p_2) into a grid with \mathcal{N} small cells, which are labeled by (i, j) with $q_2(i, j) = r_i \cos \theta_j$ and $p_2(i, j) = r_i \sin \theta_j$. Consequently, the n th eigenstate Poincaré-Husimi function is now discretized as $Q_n^P(i, j) = Q_n^P[p_2(i, j), q_2(i, j)]$ with normalization condition $\sum_{i,j} Q_n^P(i, j)/\mathcal{N} = 1$. Then, we set a quantity $C_{i,j} = +1$ to the cells that belong to the chaotic region and $C_{i,j} = -1$ for other cells. Finally, the phase space index for the n th eigenstate is defined as

$$M_n = \frac{1}{\mathcal{N}} \sum_{i,j} Q_n^P(i, j) C_{i,j}. \quad (20)$$

The definition of M_n implies that it varies in the interval $M_n \in [-1, 1]$ with $M_n = +1$ and -1 corresponding to fully chaotic and regular eigenstates, respectively. For the mixed eigenstates, as their Poincaré-Husimi functions are distributed in both chaotic and regular regions, we have $-1 < M_n < 1$. The values of M_n for the eigenstates in Fig. 4 are given in the figures. One can see that M_n is close to either $+1$ or -1 for chaotic and regular eigenstates, while it takes values between -1 and $+1$ for mixed eigenstates, as expected.

More information about the properties of the eigenstates is revealed by the probability distribution of M_n , defined as

$$P(M) = \int \rho(M) dM_n, \quad (21)$$

where $\rho(M) = \sum_n \delta(M - M_n)$ is the probability density function. It was known that $P(M)$ has two peaks at $M =$

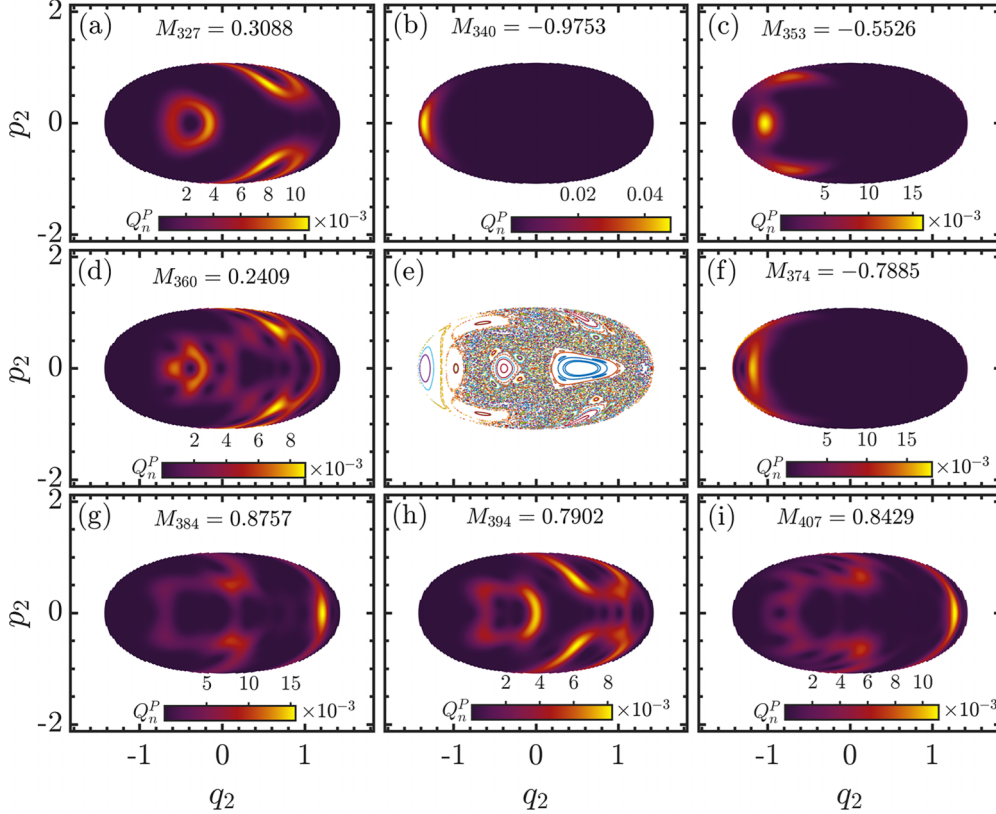


FIG. 4. Poincaré-Husimi function, $Q_n^P(p_2, q_2)$, for several positive parity eigenstates with energies (a) $E_{327}/j = -0.4391$, (b) $E_{340}/j = -0.4297$, (c) $E_{353}/j = -0.414$, (d) $E_{360}/j = -0.4067$, (f) $E_{374}/j = -0.3955$, (g) $E_{384}/j = -0.3856$, (h) $E_{394}/j = -0.3754$, and (i) $E_{407}/j = -0.3641$. Phase space overlap indices M_n , defined in Eq. (20), corresponding to these eigenstates, are given in the figure. The classical Poincaré section for $\mathcal{E} = -0.4$ is plotted in the center panel (e). Here, each color marks the points that belong to the same initial condition. Other parameters: $\omega = \omega_0 = 1$, $N = 2j = 100$, and $\lambda = 0.47$. The bosonic mode has been truncated at $\mathcal{N}_{\text{trc}} = 170$. All quantities are dimensionless.

± 1 for single particle systems [33,34], but it is necessary to perform a detailed investigation in quantum many-body systems, like the Dicke model, to see whether this property of $P(M)$ still holds. It is worth pointing out that the structure of the classical Poincaré section only depends on the coupling strength and energy. This allows us to get sufficient data for the statistics of M by considering eigenstates within an energy window for an ensemble of different system sizes. In this work, for a given energy \mathcal{E} , we will focus on the eigenstates whose energies satisfy $E_n/j \in [\mathcal{E} - \delta E, \mathcal{E} + 2\delta E]$ with $\delta E = 0.04$. We have checked that the underlying classical dynamics stays unchanged for our considered energy interval.

In Fig. 5, the distribution $P(M)$ for different system ensembles and coupling strengths, as well as energies are depicted. $P(M)$ is calculated from a finite number of eigenstates with energies within a given energy window, and plotted as the histogram. However, one can expect that it will converge to a smooth distribution in the classical limit $N \rightarrow \infty$. As seen from the figures, although $P(M)$ exhibits large fluctuations compared to the cases of single particle systems, it still behaves as a double peak distribution with two peaks located at $M \simeq \pm 1$, respectively. This is more evident for the large system sizes, as shown in Figs. 5(c), 5(f), and 5(i). The large fluctuations observed in the behaviors of $P(M)$ are due to the relative small system size, which leads to

the wide support of the Poincaré-Husimi function in the phase space. We further observe that the fluctuations in $P(M)$ can be suppressed by increasing either the system size or the degree of chaos, as revealed in single-particle systems [33,34].

The above observations of $P(M)$ suggest that larger system size N results in a sharper double peak shape of $P(M)$. Hence, one can expect that only the regular and chaotic eigenstates are left in the semiclassical limit $N \rightarrow \infty$. To strengthen this statement, we study how the relative proportion of the mixed eigenstates changes as the system size is increased. In our consideration, the mixed eigenstates are identified as the eigenstates that satisfy $-M_c \leq M \leq M_c$ with the cutoff $M_c = 0.8$. There is an arbitrariness in the choice of the value of M_c ; however, our main results are unaffected by the exact cutoff value of M_c .

The relative proportion of the mixed eigenstates is defined as

$$\mathcal{R}_m = \frac{\Delta \mathcal{N}_{\text{mix}}}{N_{\delta E}}, \quad (22)$$

where $N_{\delta E} = \sum_{E_n/j \in \delta E}$ denotes the number of eigenstates in the above mentioned energy window, while $\Delta \mathcal{N}_{\text{mix}} = \sum_{M_n \in [-M_c, M_c]}$ represents the number of mixed eigenstates in the same energy window. In Figs. 6(a) and 6(b), we show how the ensemble averaged relative proportion of the mixed

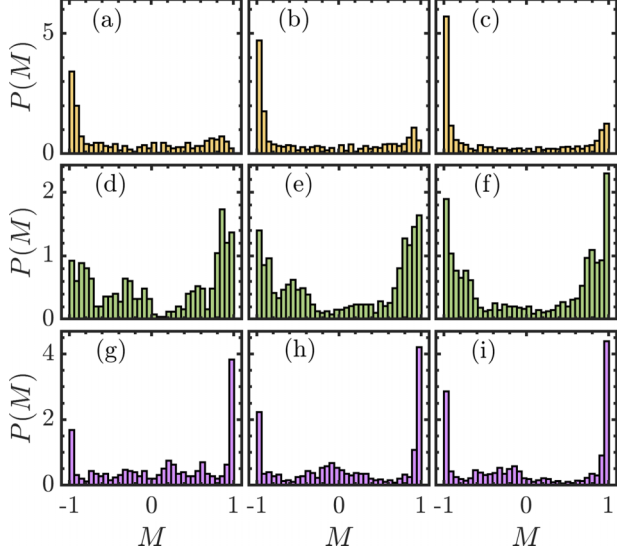


FIG. 5. (a)–(c) Probability distribution of the phase space overlap index, $P(M)$, for system size ensembles (a) $N \in [72, 88]$, (b) $N \in [92, 108]$, and (c) $N \in [112, 128]$ with $\lambda = 0.47$ and $\mathcal{E} = -0.5$. (d)–(f) $P(M)$ for the same system size ensembles and coupling strength λ as in panels (a)–(c), but for the case of $\mathcal{E} = -0.4$. (g)–(i) $P(M)$ for the same system size ensembles as in panels (a)–(c), but with $\lambda = 0.5$ and $\mathcal{E} = -0.4$. For each case, the energy of the considered eigenstates satisfies $E_n/j \in [\mathcal{E} - \delta E, \mathcal{E} + 2\delta E]$ with $\delta E = 0.04$. Other parameters: $\omega = \omega_0 = 1$. The bosonic mode has been truncated at $\mathcal{N}_{\text{trc}} = 170$. For each ensemble, the system size N is increased in steps of 4. All quantities are dimensionless.

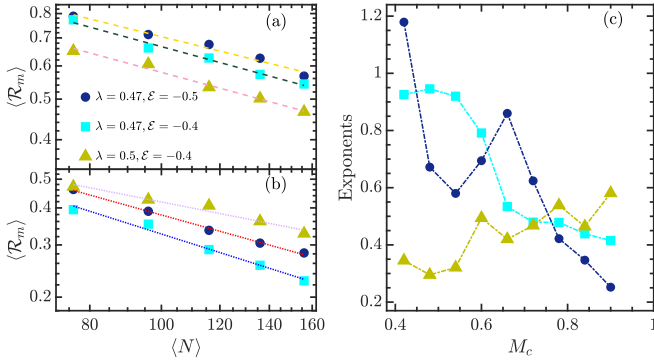


FIG. 6. (a) Ensemble averaged \mathcal{R}_m [cf. Eq. (22)] as a function of ensemble averaged system size $\langle N \rangle$ for $M_c = 0.8$ and several combinations of coupling strength λ and system energy \mathcal{E} . The dashed lines are the power-law behavior of the form $\langle \mathcal{R}_m \rangle \propto \langle N \rangle^{-\gamma}$ with $\gamma = 0.4357, 0.4797$, and 0.4779 (from top to bottom). (b) $\langle \mathcal{R}_m \rangle$ as a function of $\langle N \rangle$ for the same combinations of λ and \mathcal{E} as in panel (a) and $M_c = 0.6$. Dotted lines denote the power law $\langle \mathcal{R}_m \rangle \propto \langle N \rangle^{-\gamma}$ with $\gamma = 0.4941, 0.6944$, and 0.7913 (from top to bottom). (c) Exponents of the power-law decay as a function of M_c for the same combinations of λ and \mathcal{E} as in panels (a) and (b). For each case, the energy of the considered eigenstates satisfies $E_n/j \in [\mathcal{E} - \delta E, \mathcal{E} + 2\delta E]$ with $\delta E = 0.04$. Here, the system ensemble for each case is the same as Fig. 5 and the system size is increased in steps of 4 in each ensemble. Other parameters: $\omega = \omega_0 = 1$. The bosonic mode has been truncated at $\mathcal{N}_{\text{trc}} = 170$. All quantities are dimensionless.

eigenstates, denoted by $\langle \mathcal{R}_m \rangle$, varies as a function of ensemble averaged system size $\langle N \rangle$ for different values of M_c and several combinations of λ and \mathcal{E} . As we see in the figures, the relative proportion of the mixed eigenstates decreases with increasing system size, regardless of the values of λ and \mathcal{E} , as well as M_c . In particular, we find that the functional relationship between $\langle \mathcal{R}_m \rangle$ and $\langle N \rangle$ is well captured by the power-law decay of the form $\langle \mathcal{R}_m \rangle \propto \langle N \rangle^{-\gamma}$ with exponent γ being a function of the control parameters. Similar power-law behavior has also been observed in the single particle systems [33,34], indicating that the power-law decay of the relative proportion of the mixed eigenstates in approaching the semiclassical limit should be a universal behavior. Moreover, the decrease of \mathcal{R}_m as the system size increases is also consistent with the PUSC, and, thus, provides the evidence for the correctness of the PUSC in mixed-type many-body quantum systems. This means that a mixed-type many-body system has only fully regular and chaotic eigenstates in the ultimate semiclassical limit.

We note that the independence of our results upon the choice of M_c is confirmed by the overall power-law decay of \mathcal{R}_m for different values of M_c , as illustrated in Figs. 6(a) and 6(b). However, from the same figures, we see that the power-law exponent γ is strongly dependent on the value of M_c . This is more evident in Fig. 6(c), where we display the variation of the exponent as a function of M_c for several combinations of λ and \mathcal{E} . One can clearly see that the exponent exhibits quite large fluctuations in its behavior. This can be attributed to the fluctuations in $P(M)$ that show an obvious dependence on the choice of M_c for certain control parameters (cf. Fig. 5). As the $P(M)$ becomes smoother by increasing the level of chaos, the fluctuations in the behavior of the exponent should undergo a significant suppression for high degree of chaoticity, as exemplified in the case of $\lambda = 0.5$ and $\mathcal{E} = -0.4$.

As a final remark of this section, we would like to point out that the observed power-law decay is closely connected to flooding [113,114] and tunneling [115–118] effects in mixed systems. It is therefore necessary to perform a detailed investigation of these phenomena to understand the underlying mechanism of the power-law behavior. We leave this interesting topic for our future study. Moreover, to further verify the power-law decay as a universal property of the fraction of the mixed eigenstates, it is also necessary to examine how the fraction of the mixed eigenstates varies in many-body quantum systems that have no classical counterpart, such as different spin models. However, how to identify the types of eigenstates in such systems remains unknown and is beyond the scope of the present work; we take it as one of our future directions.

IV. CONCLUSIONS

A basic and valuable tool for comprehending various characters of general mixed quantum systems is the principle of uniform semiclassical condensation of Wigner or Husimi functions (PUSC) [22–24]. Although the validity of the PUSC in the mixed-type single-particle systems has been verified by numerous works, its correctness for the mixed-type many-body quantum systems remains unknown. With the aim to

address this question, we have delved into a detailed analysis of the eigenstates and their properties in the celebrated Dicke model. As a prototypical model in the studies of both quantum and classical chaos, the Dicke model is a very suitable many-body quantum model for our study because it attains its well defined semiclassical limit as the system size is increased. Hence, the Dicke model allows us to define an effective Planck constant, which is essential to explore how the features of eigenstates change as the semiclassical limit is approached.

By investigating the development of chaos in both classical and quantum Dicke models, we have determined the parameter and energy regions that exhibit the mixed-type behavior. By means of Husimi function, we have shown that the eigenstates can be divided into different types. To quantitatively characterize different types of eigenstates, we have calculated the phase space overlap index, which is defined in terms of the Husimi function and acts as a useful tool for studying the characters of the eigenstates. For the eigenstates that belong to a certain classical dynamical regime, the distribution of their phase space overlap index is well described by double peak distribution with two peaks at -1 and $+1$, corresponding to the fully regular and chaotic eigenstates, respectively. For finite system size, there are many mixed eigenstates with the value of phase space overlap index varying between -1 and $+1$. However, we have shown that the relative proportion of the mixed eigenstates vanishes with increasing system size, i.e., approaching the semiclassical limit. This means that the eigenstates in the mixed-type many-body quantum systems belong to either regular or chaotic type as the semiclassical limit is approached, as we have observed similarly in the

single-particle systems [33,34] and in accord with the PUSC. In particular, we have demonstrated that the decay of the relative proportion of the mixed eigenstates with increasing system size is well captured by a power law, similar to the results obtained in the single-particle systems. This leads us to believe that the power-law decay is a universal behavior in the evolution of the relative proportion of the mixed eigenstates in mixed-type systems as the semiclassical limit is approached.

An interesting extension of the present work is to explore the validity of PUSC in many-body quantum systems that have no classical correspondence, such as various quantum spin systems. The lack of classical counterpart indicates that new methods should be found to identify the types of eigenstates. A possible candidate to fulfill this requirement might be the entanglement entropy of the eigenstates; however, we leave this subtle question for our future investigation. In addition, a theoretical understanding of the properties exhibited by the mixed eigenstates in many-body quantum systems also deserves future exploration. Finally, we hope that our work could motivate more studies of the features of the mixed-type many-body quantum systems.

ACKNOWLEDGMENTS

This work was supported by the Slovenian Research and Innovation Agency (ARIS) under Grants No. J1-4387 and No. P1-0306. Q.W. acknowledges support from the National Science Foundation of China (NSFC) under Grant No. 11805165 and the Zhejiang Provincial Nature Science Foundation under Grant No. LY20A05001.

-
- [1] L. Vidmar and M. Rigol, *Phys. Rev. Lett.* **119**, 220603 (2017).
 - [2] C. Murthy and M. Srednicki, *Phys. Rev. E* **100**, 022131 (2019).
 - [3] M. Haque, P. A. McClarty, and I. M. Khaymovich, *Phys. Rev. E* **105**, 014109 (2022).
 - [4] B. Batistić and M. Robnik, *J. Phys. A: Math. Theor.* **46**, 315102 (2013).
 - [5] B. Batistić, Č. Lozej, and M. Robnik, *Phys. Rev. E* **100**, 062208 (2019).
 - [6] B. Batistić, Č. Lozej, and M. Robnik, *Nonlinear Phenom. Complex Syst.* **23**, 17 (2020).
 - [7] Q. Wang and M. Robnik, *Phys. Rev. E* **107**, 054213 (2023).
 - [8] Q. Wang and M. Robnik, *Phys. Rev. E* **102**, 032212 (2020).
 - [9] D. Villaseñor, S. Pilatowsky-Cameo, M. A. Bastarrachea-Magnani, S. Lerma-Hernández, and J. G. Hirsch, *Phys. Rev. E* **103**, 052214 (2021).
 - [10] S. Pilatowsky-Cameo, D. Villaseñor, M. A. Bastarrachea-Magnani, S. Lerma-Hernández, L. F. Santos, and J. G. Hirsch, *New J. Phys.* **23**, 033045 (2021).
 - [11] S. Pilatowsky-Cameo, D. Villaseñor, M. A. Bastarrachea-Magnani, S. Lerma-Hernández, L. F. Santos, and J. G. Hirsch, *Quantum* **6**, 644 (2022).
 - [12] A. Chandran, T. Iadecola, V. Khemani, and R. Moessner, *Annu. Rev. Condens. Matter Phys.* **14**, 443 (2023).
 - [13] B. Evrard, A. Pizzi, S. I. Mistakidis, and C. B. Dag, *Phys. Rev. Lett.* **132**, 020401 (2024).
 - [14] A. Bäcker, M. Haque, and I. M. Khaymovich, *Phys. Rev. E* **100**, 032117 (2019).
 - [15] L. Pausch, E. G. Carnio, A. Rodríguez, and A. Buchleitner, *Phys. Rev. Lett.* **126**, 150601 (2021).
 - [16] M. A. Bastarrachea-Magnani, D. Villaseñor, J. Chávez-Carlos, S. Lerma-Hernández, L. F. Santos, and J. G. Hirsch, [arXiv:2307.03801](https://arxiv.org/abs/2307.03801).
 - [17] M. Kourehpaz, S. Donsa, F. Lackner, J. Burgdörfer, and I. Březinová, *Entropy* **24**, 1740 (2022).
 - [18] G. Nakerst and M. Haque, *Phys. Rev. E* **107**, 024210 (2023).
 - [19] I. C. Percival, *J. Phys. B: At. Mol. Phys.* **6**, L229 (1973).
 - [20] M. V. Berry, *J. Phys. A: Math. Gen.* **10**, 2083 (1977).
 - [21] M. V. Berry and J. M. Ziman, *Philos. Trans. R. Soc. London. Ser. A, Math. Phys. Sci.* **287**, 237 (1977).
 - [22] M. Robnik, *Nonlinear Phenom. Complex Syst.* **1**, 1 (1998).
 - [23] M. Robnik, Recent advances in quantum chaos of generic systems, in *Encyclopedia of Complexity and Systems Science*, edited by R. A. Meyers (Springer, Berlin, 2019), pp. 1–17.
 - [24] M. Robnik, *Nonlinear Phenom. Complex Syst.* **23**, 172 (2020).
 - [25] T. Prosen and M. Robnik, *J. Phys. A: Math. Gen.* **26**, 5365 (1993).
 - [26] G. Veble, M. Robnik, and J. Liu, *J. Phys. A: Math. Gen.* **32**, 6423 (1999).

- [27] M. V. Berry and M. Robnik, *J. Phys. A: Math. Gen.* **17**, 2413 (1984).
- [28] T. Prosen and M. Robnik, *J. Phys. A: Math. Gen.* **27**, L459 (1994).
- [29] B. Li and M. Robnik, *J. Phys. A: Math. Gen.* **27**, 5509 (1994).
- [30] B. Li and M. Robnik, *J. Phys. A: Math. Gen.* **28**, 4843 (1995).
- [31] T. Prosen and M. Robnik, *J. Phys. A: Math. Gen.* **32**, 1863 (1999).
- [32] T. Manos and M. Robnik, *Phys. Rev. E* **87**, 062905 (2013).
- [33] Č. Lozej, D. Lukman, and M. Robnik, *Phys. Rev. E* **106**, 054203 (2022).
- [34] Q. Wang and M. Robnik, *Phys. Rev. E* **108**, 054217 (2023).
- [35] R. H. Dicke, *Phys. Rev.* **93**, 99 (1954).
- [36] K. Hepp and E. H. Lieb, *Phys. Rev. A* **8**, 2517 (1973).
- [37] K. Hepp and E. H. Lieb, *Ann. Phys. (NY)* **76**, 360 (1973).
- [38] P. Kirton, M. M. Roses, J. Keeling, and E. G. Dalla Torre, *Adv. Quantum Technol.* **2**, 1800043 (2019).
- [39] P. Pérez-Fernández and A. Relaño, *Phys. Rev. E* **96**, 012121 (2017).
- [40] P. Das and A. Sharma, *Phys. Rev. A* **105**, 033716 (2022).
- [41] V. M. Bastidas, C. Emary, B. Regler, and T. Brandes, *Phys. Rev. Lett.* **108**, 043003 (2012).
- [42] D. Nagy, G. Kónya, G. Szirmai, and P. Domokos, *Phys. Rev. Lett.* **104**, 130401 (2010).
- [43] K. Baumann, C. Guerlin, F. Brennecke, and T. Esslinger, *Nature (London)* **464**, 1301 (2010).
- [44] K. Baumann, R. Mottl, F. Brennecke, and T. Esslinger, *Phys. Rev. Lett.* **107**, 140402 (2011).
- [45] E. Romera, R. del Real, and M. Calixto, *Phys. Rev. A* **85**, 053831 (2012).
- [46] C. Emary and T. Brandes, *Phys. Rev. Lett.* **90**, 044101 (2003).
- [47] C. Emary and T. Brandes, *Phys. Rev. E* **67**, 066203 (2003).
- [48] P. Pérez-Fernández, A. Relaño, J. M. Arias, P. Cejnar, J. Dukelsky, and J. E. García-Ramos, *Phys. Rev. E* **83**, 046208 (2011).
- [49] M. A. Bastarrachea-Magnani, S. Lerma-Hernández, and J. G. Hirsch, *Phys. Rev. A* **89**, 032101 (2014).
- [50] C. M. Lóbez and A. Relaño, *Phys. Rev. E* **94**, 012140 (2016).
- [51] T. Brandes, *Phys. Rev. E* **88**, 032133 (2013).
- [52] R. Puebla and A. Relaño, *Europhys. Lett.* **104**, 50007 (2013).
- [53] A. L. Corps and A. Relaño, *Phys. Rev. Lett.* **127**, 130602 (2021).
- [54] M. A. Bastarrachea-Magnani, S. Lerma-Hernández, and J. G. Hirsch, *Phys. Rev. A* **89**, 032102 (2014).
- [55] M. A. Bastarrachea-Magnani, B. L. del Carpio, S. Lerma-Hernández, and J. G. Hirsch, *Phys. Scr.* **90**, 068015 (2015).
- [56] J. Chávez-Carlos, M. A. Bastarrachea-Magnani, S. Lerma-Hernández, and J. G. Hirsch, *Phys. Rev. E* **94**, 022209 (2016).
- [57] L. Song, D. Yan, J. Ma, and X. Wang, *Phys. Rev. E* **79**, 046220 (2009).
- [58] U. Bhattacharya, S. Dasgupta, and A. Dutta, *Phys. Rev. E* **90**, 022920 (2014).
- [59] S. Lerma-Hernández, D. Villaseñor, M. A. Bastarrachea-Magnani, E. J. Torres-Herrera, L. F. Santos, and J. G. Hirsch, *Phys. Rev. E* **100**, 012218 (2019).
- [60] J. Chávez-Carlos, B. López-del-Carpio, M. A. Bastarrachea-Magnani, P. Stránský, S. Lerma-Hernández, L. F. Santos, and J. G. Hirsch, *Phys. Rev. Lett.* **122**, 024101 (2019).
- [61] A. Altland and F. Haake, *Phys. Rev. Lett.* **108**, 073601 (2012).
- [62] A. Altland and F. Haake, *New J. Phys.* **14**, 073011 (2012).
- [63] R. J. Lewis-Swan, A. Safavi-Naini, J. J. Bollinger, and A. M. Rey, *Nat. Commun.* **10**, 1581 (2019).
- [64] C. M. Lóbez and A. Relaño, *J. Stat. Mech.* (2021) 083104.
- [65] S. Pilatowsky-Cameo, D. Villaseñor, M. A. Bastarrachea-Magnani, S. Lerma-Hernández, L. F. Santos, and J. G. Hirsch, *Nat. Commun.* **12**, 852 (2021).
- [66] D. Villaseñor, S. Pilatowsky-Cameo, M. A. Bastarrachea-Magnani, S. Lerma-Hernández, L. F. Santos, and J. G. Hirsch, *Entropy* **25**, 8 (2023).
- [67] M. Caprio, P. Cejnar, and F. Iachello, *Ann. Phys. (NY)* **323**, 1106 (2008).
- [68] P. Stránský, M. Macek, and P. Cejnar, *Ann. Phys. (NY)* **345**, 73 (2014).
- [69] P. Cejnar, P. Stránský, M. Macek, and M. Kloc, *J. Phys. A: Math. Theor.* **54**, 133001 (2021).
- [70] R. Puebla, A. Relaño, and J. Retamosa, *Phys. Rev. A* **87**, 023819 (2013).
- [71] J. M. Radcliffe, *J. Phys. A: Gen. Phys.* **4**, 313 (1971).
- [72] W.-M. Zhang, D. H. Feng, and R. Gilmore, *Rev. Mod. Phys.* **62**, 867 (1990).
- [73] M. de Aguiar, K. Furuya, C. Lewenkopf, and M. Nemes, *Ann. Phys. (NY)* **216**, 291 (1992).
- [74] L. Bakemeier, A. Alvermann, and H. Fehske, *Phys. Rev. A* **88**, 043835 (2013).
- [75] Note that these definitions are somewhat different from our previous work [8], basically by a rescaling factor 2, and therefore are canonically equivalent.
- [76] C. Skokos, The Lyapunov characteristic exponents and their computation, in *Dynamics of Small Solar System Bodies and Exoplanets*, edited by J. J. Souchay and R. Dvorak (Springer, Berlin, 2010), pp. 63–135.
- [77] A. Lichtenberg and M. Leiberman, *Regular and Chaotic Dynamics*, Applied Mathematical Sciences (Springer, New York, 2013).
- [78] O. Bohigas, M. J. Giannoni, and C. Schmit, *Phys. Rev. Lett.* **52**, 1 (1984).
- [79] F. M. Izrailev, *Phys. Rep.* **196**, 299 (1990).
- [80] K. Zyczkowski, *J. Phys. A: Math. Gen.* **23**, 4427 (1990).
- [81] J. M. G. Gómez, K. Kar, V. Kota, R. Molina, A. Relaño, and J. Retamosa, *Phys. Rep.* **499**, 103 (2011).
- [82] F. Haake, S. Gnutzmann, and M. Kuś, *Quantum Signatures of Chaos*, Springer Series in Synergetics (Springer International, Cham, 2019).
- [83] F. Borgonovi, F. Izrailev, L. Santos, and V. Zelevinsky, *Phys. Rep.* **626**, 1 (2016).
- [84] T. Gorin, T. Prosen, T. H. Seligman, and M. Žnidarič, *Phys. Rep.* **435**, 33 (2006).
- [85] A. Bhattacharyya, W. Chemissany, S. S. Haque, and B. Yan, *Eur. Phys. J. C* **82**, 87 (2022).
- [86] D. E. Parker, X. Cao, A. Avdoshkin, T. Scaffidi, and E. Altman, *Phys. Rev. X* **9**, 041017 (2019).
- [87] A. Dymarsky and A. Gorsky, *Phys. Rev. B* **102**, 085137 (2020).
- [88] A. Bhattacharyya, W. Chemissany, S. S. Haque, J. Murugan, and B. Yan, *SciPost Phys. Core* **4**, 002 (2021).
- [89] A. Bhattacharyya, S. S. Haque, and E. H. Kim, *J. High Energy Phys.* **10** (2021) 028.
- [90] V. Balasubramanian, P. Caputa, J. M. Magan, and Q. Wu, *Phys. Rev. D* **106**, 046007 (2022).

- [91] B. L. Español and D. A. Wisniacki, *Phys. Rev. E* **107**, 024217 (2023).
- [92] K. Hashimoto, K. Murata, N. Tanahashi, and R. Watanabe, *J. High Energy Phys.* **11** (2023) 040.
- [93] V. Oganesyan and D. A. Huse, *Phys. Rev. B* **75**, 155111 (2007).
- [94] Y. Y. Atas, E. Bogomolny, O. Giraud, and G. Roux, *Phys. Rev. Lett.* **110**, 084101 (2013).
- [95] A. L. Corps and A. Relaño, *Phys. Rev. E* **101**, 022222 (2020).
- [96] L. Sá, P. Ribeiro, and T. Prosen, *Phys. Rev. X* **10**, 021019 (2020).
- [97] P. Łydźba and T. Sowiński, *Phys. Rev. A* **106**, 013301 (2022).
- [98] O. Giraud, N. Macé, E. Vernier, and F. Alet, *Phys. Rev. X* **12**, 011006 (2022).
- [99] M. Robnik, *Eur. Phys. J. Spec. Top.* **225**, 959 (2016).
- [100] E. Wigner, *Phys. Rev.* **40**, 749 (1932).
- [101] K. Husimi, *Proc. Phys. Math. Soc. Jpn* **22**, 264 (1940).
- [102] M. B. Cibils, Y. Cuche, P. Leboeuf, and W. F. Wreszinski, *Phys. Rev. A* **46**, 4560 (1992).
- [103] I. Oregi and F. J. Arranz, *Phys. Rev. E* **89**, 022909 (2014).
- [104] S. Sinha and S. Sinha, *Phys. Rev. Lett.* **125**, 134101 (2020).
- [105] D. Mondal, S. Sinha, and S. Sinha, *Phys. Rev. E* **102**, 020101(R) (2020).
- [106] Q. Wang and M. Robnik, *Entropy* **23** (2021).
- [107] K. Takahashi, *J. Phys. Soc. Jpn.* **55**, 762 (1986).
- [108] M. A. M. de Aguiar, K. Furuya, C. H. Lewenkopf, and M. C. Nemes, *Europhys. Lett.* **15**, 125 (1991).
- [109] K. Furuya, M. de Aguiar, C. Lewenkopf, and M. Nemes, *Ann. Phys. (NY)* **216**, 313 (1992).
- [110] P. Leboeuf and M. Saraceno, *J. Phys. A: Math. Gen.* **23**, 1745 (1990).
- [111] G. Groh, H. J. Korsch, and W. Schweizer, *J. Phys. A: Math. Gen.* **31**, 6897 (1998).
- [112] M. A. Bastarrachea-Magnani, B. López-del-Carpio, J. Chávez-Carlos, S. Lerma-Hernández, and J. G. Hirsch, *Phys. Rev. E* **93**, 022215 (2016).
- [113] A. Bäcker, R. Ketzmerick, and A. G. Monastera, *Phys. Rev. Lett.* **94**, 054102 (2005).
- [114] A. Bäcker, R. Ketzmerick, and A. G. Monastera, *Phys. Rev. E* **75**, 066204 (2007).
- [115] A. Bäcker, R. Ketzmerick, S. Löck, and L. Schilling, *Phys. Rev. Lett.* **100**, 104101 (2008).
- [116] A. Bäcker, R. Ketzmerick, S. Löck, M. Robnik, G. Vidmar, R. Höhmann, U. Kuhl, and H.-J. Stöckmann, *Phys. Rev. Lett.* **100**, 174103 (2008).
- [117] V. A. Podolskiy and E. E. Narimanov, *Phys. Rev. Lett.* **91**, 263601 (2003).
- [118] S. Tomsovic, *Phys. Scr.* **2001**, 162 (2001).